Supplementary Information

Spin-orbit coupling effects hidden behind the photophysics of phosphorescent chiral cyclometalated Pt(II) complexes

Thomas Groizard, Souvik Mandal, Christophe Gourlaouen,[§] Chantal Daniel*

	Complex **1**	Complex **2**
Pt-O_1 (Å)	2.129	2.115
Pt-O_2 (Å)	2.035	2.019
Pt-C (Å)	2.010	2.020
Pt-N (Å)	2.008	1.982
CCCC (°)	57.8	59.4

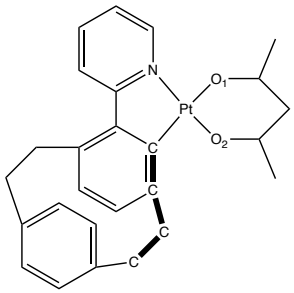

Figure S1. Selected optimized structural parameters of complexes **1** and **2**.

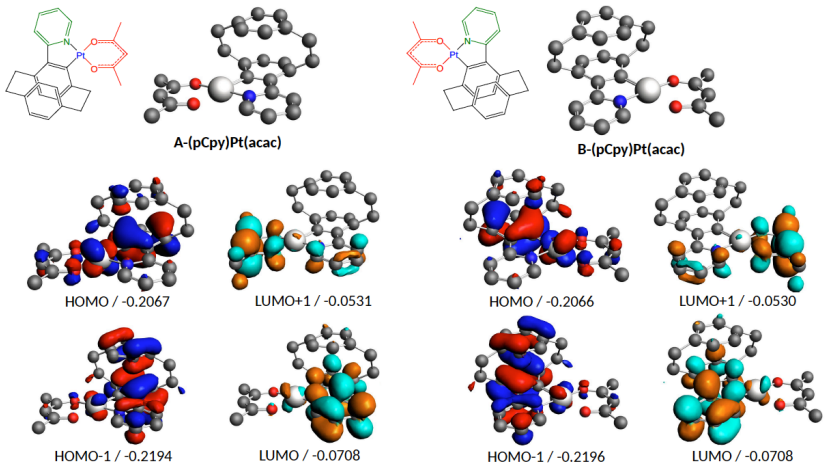

Figure S2. DFT frontier Kohn-Sham orbitals of complex **1**.

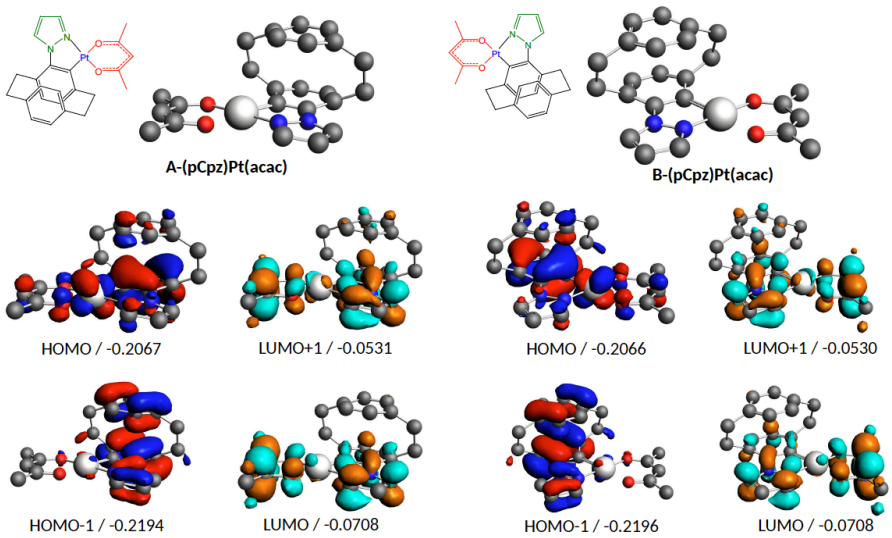

Figure S3. DFT frontier Kohn-Sham orbitals of complex **2**.

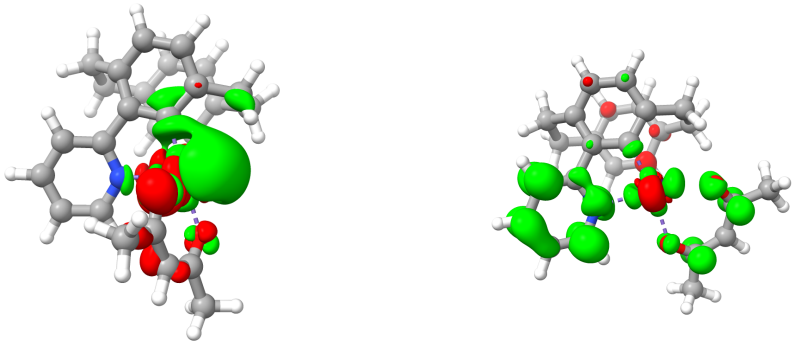

Figure S4. Difference in electronic densities describing the metal-centred MC1 and MC2 low-lying triplet states in complex **1** enantiomer A (in green: gain of electronic density, in red: loss of density).

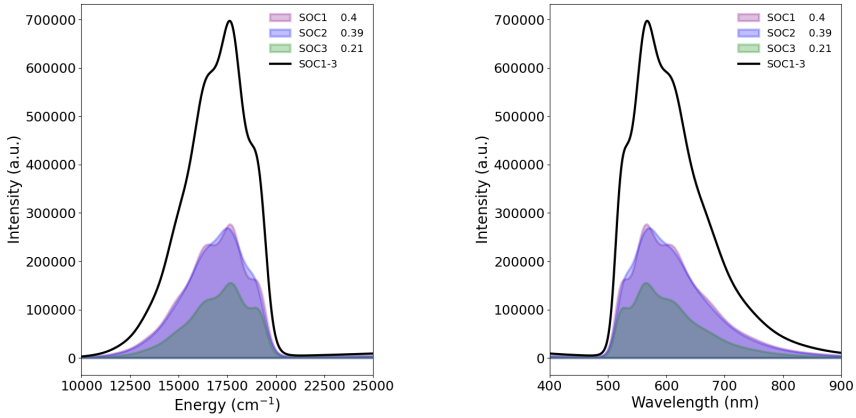

Figure S5. Calculated phosphorescence spectrum of complex **2** enantiomer A at room temperature.

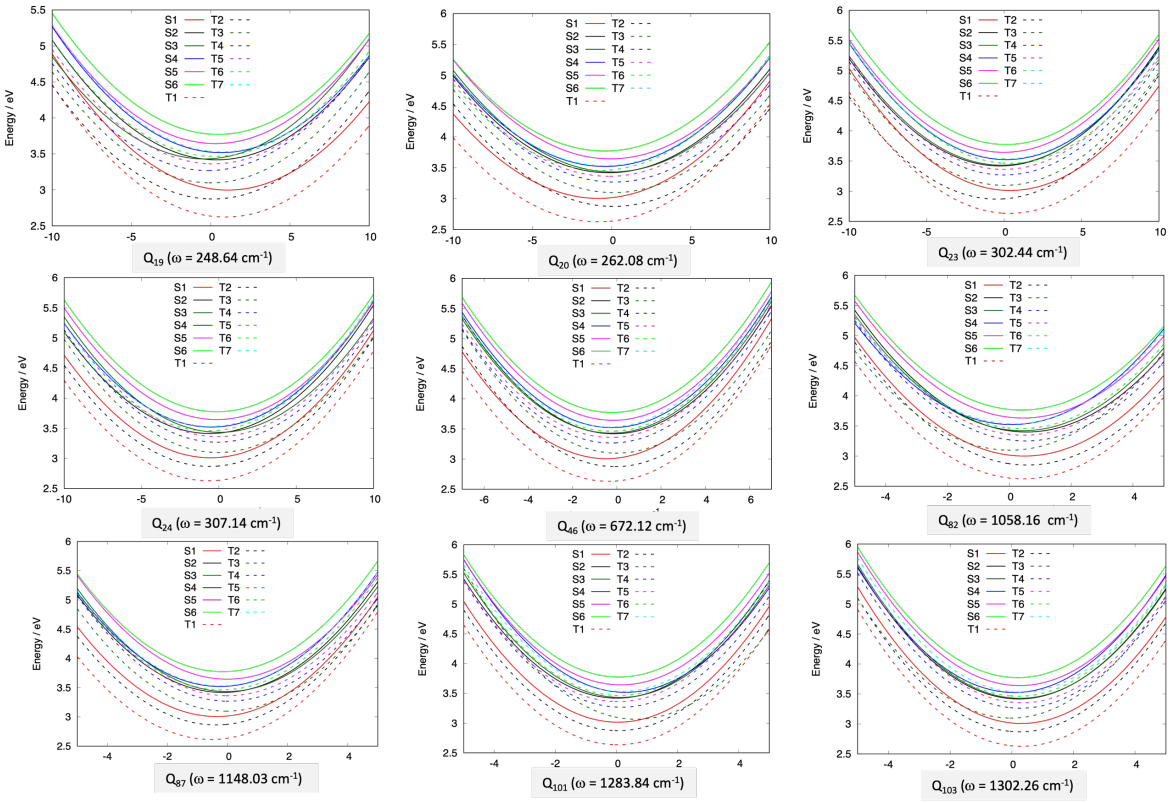
S1 T2
S2 T3
S3 T4
S4 T5
S5 T6
S6 T7
T1
Energy / eV
Q19 (ω = 248.64 cm-1)
Q20 (ω = 262.08 cm-1)
Q23 (ω = 302.44 cm-1)
Q24 (ω = 307.14 cm-1)
Q46 (ω = 672.12 cm-1)
Q82 (ω = 1058.16 cm-1)
Q87 (ω = 1148.03 cm-1)
Q101 (ω = 1283.84 cm-1)
Q103 (ω = 1302.26 cm-1)

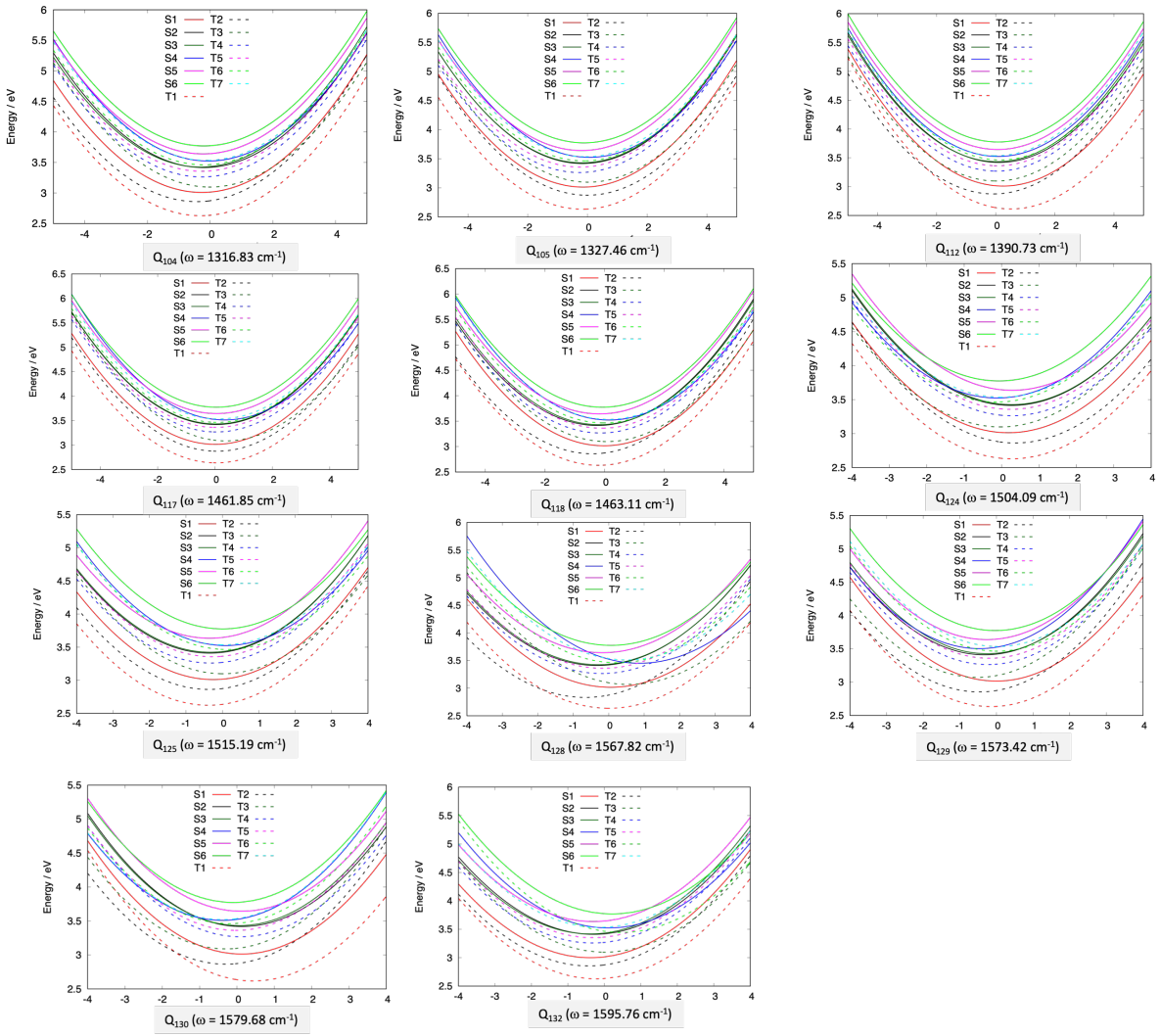

Figure S6. One-Dim cuts of the PES of complex **1** as function of the 20 active normal modes selected in the quantum dynamics simulation.

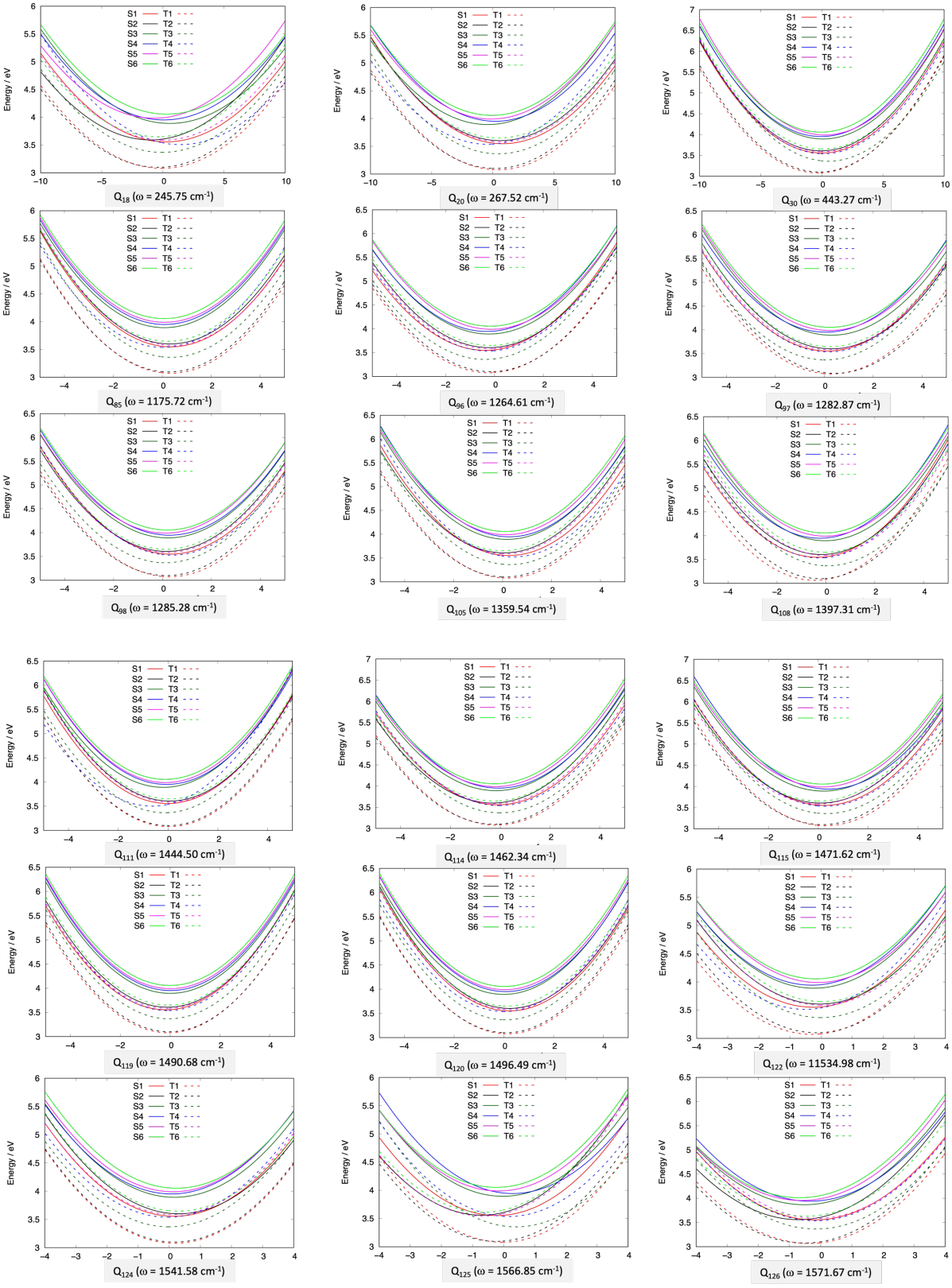
S1 T1
S2 T2
S3 T3
S4 T4
S5 T5
S6 T6
Energy / eV
Q18 (ω = 245.75 cm-1)
Q20 (ω = 267.52 cm-1)
Q30 (ω = 443.27 cm-1)
Q85 (ω = 1175.72 cm-1)
Q96 (ω = 1264.61 cm-1)
Q97 (ω = 1282.87 cm-1)
Q98 (ω = 1285.28 cm-1)
Q105 (ω = 1359.54 cm-1)
Q108 (ω = 1397.31 cm-1)
Q111 (ω = 1444.50 cm-1)
Q114 (ω = 1462.34 cm-1)
Q115 (ω = 1471.62 cm-1)
Q119 (ω = 1490.68 cm-1)
Q120 (ω = 1496.49 cm-1)
Q122 (ω = 11534.98 cm-1)
Q124 (ω = 1541.58 cm-1)
Q125 (ω = 1566.85 cm-1)
Q126 (ω = 1571.67 cm-1)

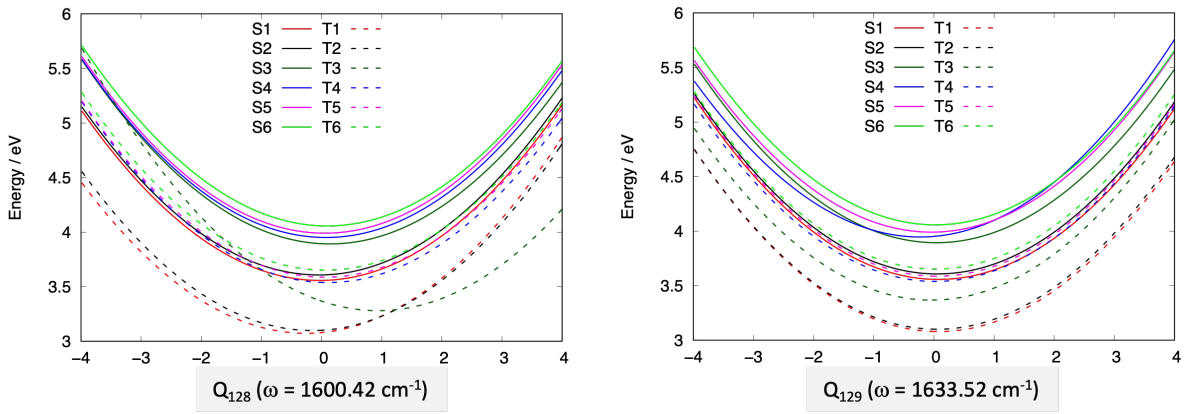

Figure S7. One-Dim cuts of the PES of complex **2** as function of the 20 active normal modes selected in the quantum dynamics simulation. (The associated frequencies in cm^{-1} are given in abscise)

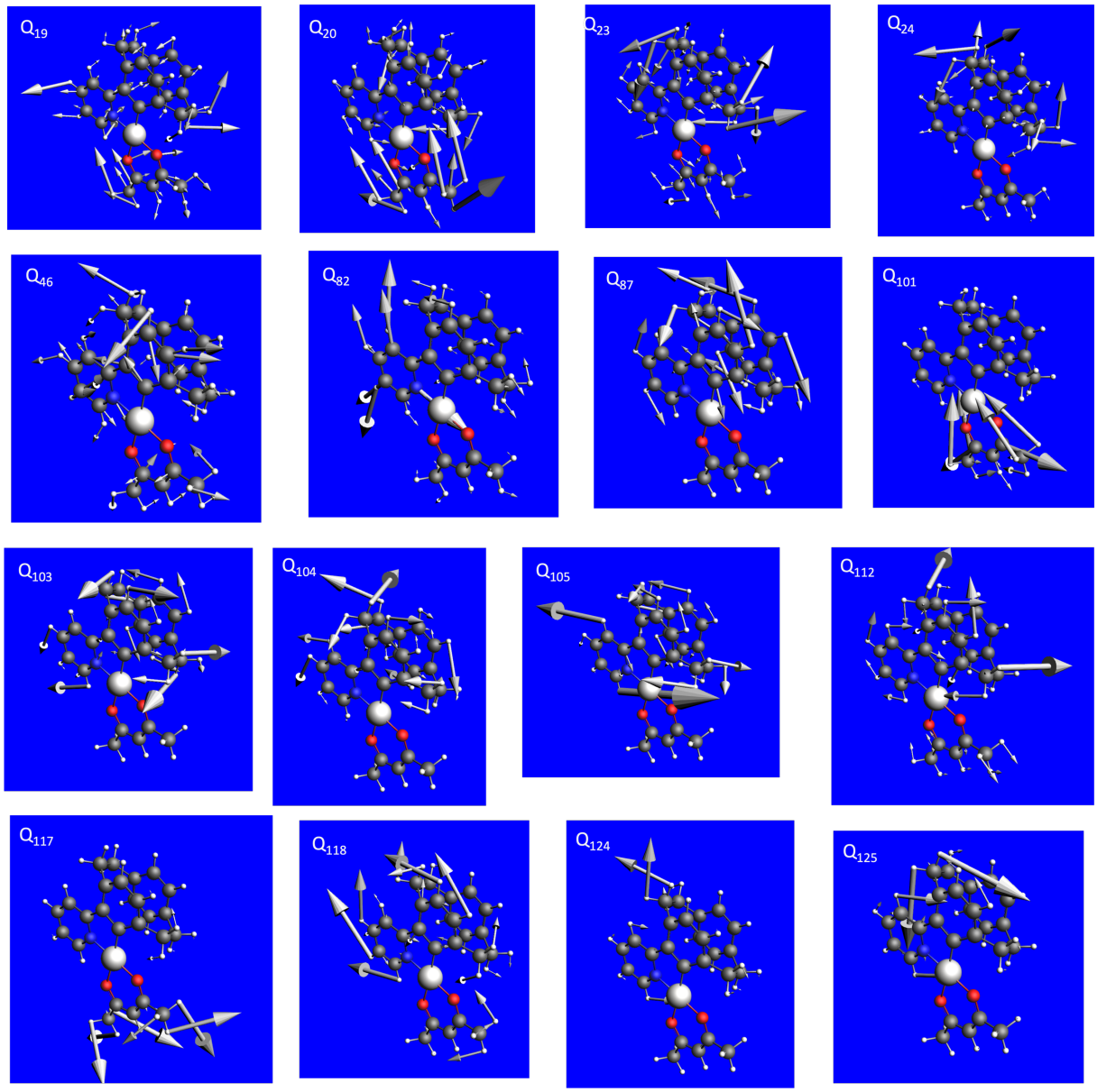

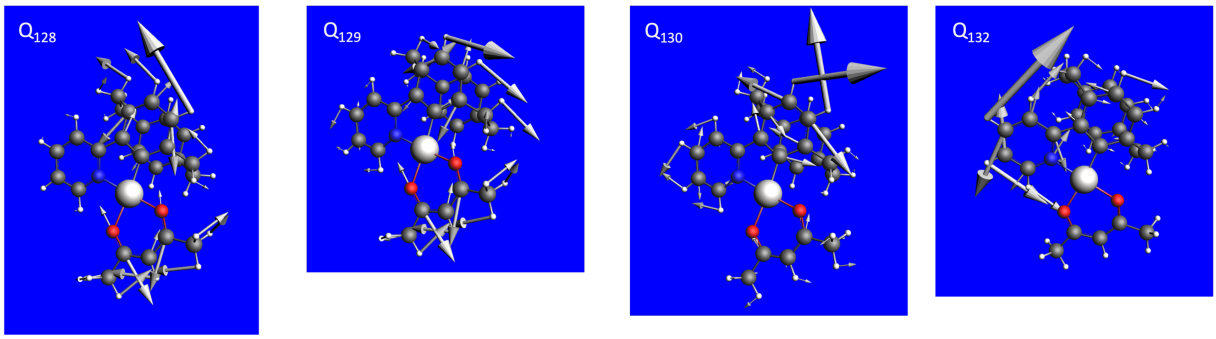

Figure S8. Selected normal modes in the QD simulation for Complex **1**.

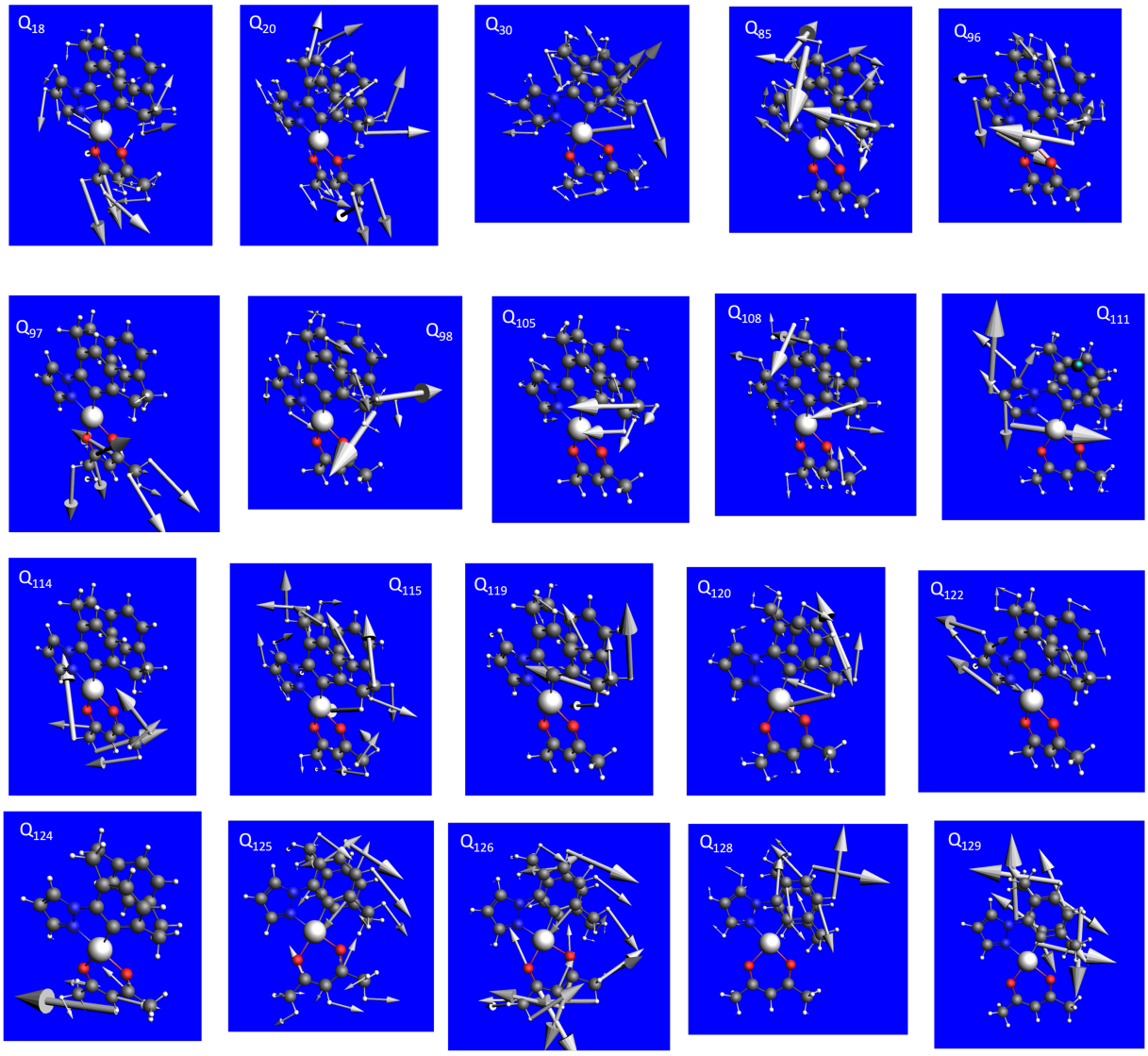

Figure S9. Selected normal modes in the QD simulation for Complex **2**.

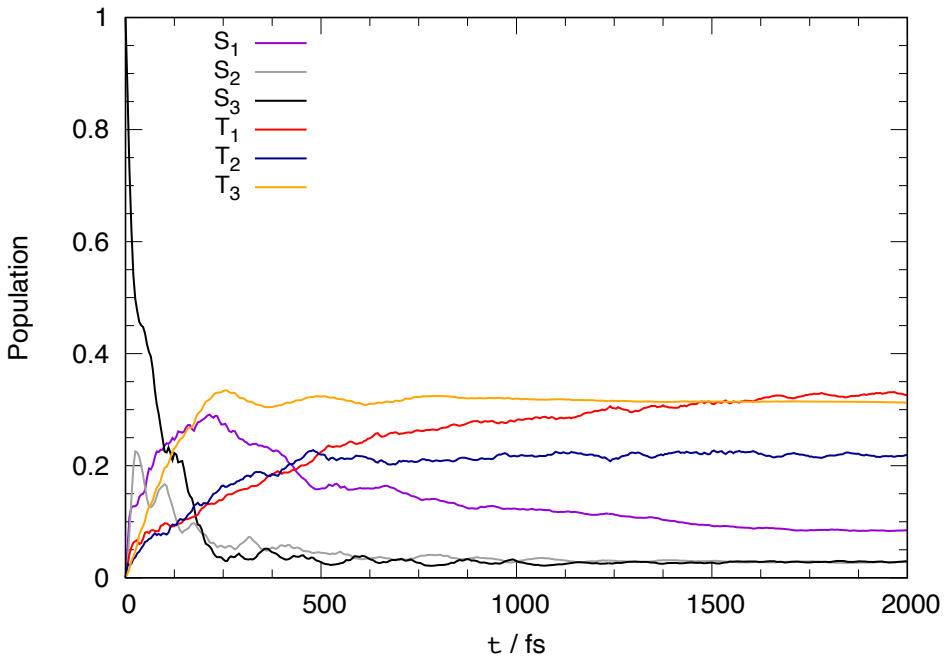

Figure S10. Time-evolution of the diabatic populations of the low-lying excited states of complexes **1** within 2 ps. The diabatic population for the T_n states represents the sum over the three SO sublevels.

Table S1. Experimental absorption data from reference 35.

	λ^{max}(nm)	$\varepsilon(10^4)$		λ^{max}(nm)	$\varepsilon(10^4)$
Complex **1**	275	2.3	Complex **2**	278	1.3
	332	1.2		316	0.82
	355	0.82		370	0.36
	378	0.75			
	434	0.35			

Table S2. Calculated transition electric and magnetic dipoles (in a. u.) for each SO sublevel E1, E2, E3 of the T1a state of complex 1. SOC1, SOC2, SOC3 means E1, E2 and E3, respectively.

magn

Re X	Im X	Re Y	Im Y	Re Z	Im Z
0.00044	-0.00443	-0.00018	0.00185	0.00012	-0.00118
-0.01094	-0.01438	-0.0025	-0.00329	0.00069	0.00091
-0.00770	-0.00677	-0.00333	-0.00293	-0.01262	-0.01111

elec

Re X	Im X	Re Y	Im Y	Re Z	Im Z
0.00307	0.0003	0.03553	0.00351	-0.01938	-0.00191
0.0151	-0.01148	0.01396	-0.01061	-0.00364	0.00277
0.03755	-0.04267	-0.04379	0.04977	0.00273	-0.0031

TRANSITION MAGNETIC DIPOLE MOMENTS

SOC1	0,00044-0,00443i	-0,00018+0,00185i	0,00012-0,00118i
SOC2	-0,01094-0,01438i	-0,0025-0,00329i	0,00069+0,00091i
SOC3	-0,0077-0,00677i	-0,00333-0,00293i	-0,01262-0,01111i

TRANSITION MAGNETIC DIPOLE MOMENTS CONJUG.

SOC1	0,00044+0,00443i	-0,00018-0,00185i	0,00012+0,00118i
SOC2	-0,01094+0,01438i	-0,0025+0,00329i	0,00069-0,00091i
SOC3	-0,0077+0,00677i	-0,00333+0,00293i	-0,01262+0,01111i

TRANSITION ELECTRIC DIPOLE MOMENTS

SOC1	0,00307+0,0003i	0,03553+0,00351i	-0,01938-0,00191i
SOC2	0,0151-0,01148i	0,01396-0,01061i	-0,00364+0,00277i
SOC3	0,03755-0,04267i	-0,04379+0,04977i	0,00273-0,0031i

SCALAR PRODUCT

SOC1	4,81000000000009e-08-7,57278e-05i
SOC2	-9,559999999999724e-08+0,0004204063i
SOC3	-2,760999999999989e-07+0,000358186i

IMAGINARY PART			**compar R**
	ua	**10^40 cgs**	**10^40 cgs**
SOC1	-7.573E-05	-3.570E-02	-3.573E-02
SOC2	4.204E-04	1.982E-01	1.982E-01
SOC3	3.582E-04	1.689E-01	1.688E-01

Table S3. SOC (in cm^{-1}) between the 3 lowest singlet and triplet states as used in the *W(Q)* coupling matrix.

Complex **1**						
	T1		T2		T3	
	real	imaginary	real	imaginary	real	imaginary
S1	21.661	−60.793	86.833	−233.030	−10.716	−16.417
S2	−263.240	191.120	80.467	60.067	22.643	14.6120
S3	260.470	−669.070	−198.040	−217.620	−15.425	−88.686
T1			77.219	163.610	−6.087	81.080
T2					7.740	40.489
Complex **2**						
	T1		T2		T3	
	real	imaginary	real	imaginary	real	imaginary
S1	41.070	150.240	6.098	14.656	−11.337	142.250
S2	3.065	−143.610	−72.294	−191.960	27.568	93.893
S3	68.819	610.750	42.410	63.350	35.343	248.600
T1			9.761	54.862	31.553	−43.396
T2					−44.656	−54.052

Table S4. Selected intra-state coupling elements κ_i^n (in eV and > 0.02 eV) and associated Q_i normal modes and frequencies ω_i (in cm^{-1}).

Complex **1**	ω_i	κ^{S1}	κ^{S2}	κ^{S3}	κ^{T1}	κ^{T2}	κ^{T3}
Q_{19}	248.64	-.0332			-0.0284		
Q_{20}	262.08	0.0268			0.0272		
Q_{23}	302.44						
Q_{24}	307.14	0.0206	0.0223		0.0245	0.0232	
Q_{46}	672.12	0.0393		0.0209	0.0307		
Q_{82}	1058.16	-0.0629	-0.0726		-0.0593	-0.0757	
Q_{87}	1148.03	0.0513	0.0229		0.0774	0.0556	
Q_{101}	1283.84			-0.0202			-0.1027
Q_{103}	1302.26	-0.050	-0.0365	-0.0425	-0.0510	-0.0414	
Q_{104}	1316.83	0.0431	0.0337	0.050	0.0491	0.070	
Q_{105}	1327.46	0.0213	0.0273	0.0302	0.0268		

Q_{112}	1390.73	-0.0431			-0.0884		
Q_{117}	1461.85						-0.0678
Q_{118}	1463.11		0.0432	0.0329	0.0356	0.0746	
Q_{124}	1504.09	-0.0336	-0.0483	-0.0511	-0.0501	-0.0674	
Q_{125}	1515.19	0.0462	0.0649	0.0626	0.0715	0.0702	
Q_{128}	1567.82		0.0637	0.0582		0.1283	-0.110
Q_{129}	1573.42		0.0626	0.0495	0.0296	0.0912	0.1025
Q_{130}	1579.68	-0.0250	-0.0246		-0.0843	0.0595	0.0565
Q_{132}	1585.76	0.0759	0.0584	0.0756	0.0439	0.0850	
Complex **2**	ω_i	κ^{S1}	κ^{S2}	κ^{S3}	κ^{T1}	κ^{T2}	κ^{T3}
Q_{18}	245.75		0.0309				
Q_{20}	267.52	-0.0266					
Q_{30}	443.27						-0.0291
Q_{85}	1175.72		-0.0471		-0.0492	-0.0389	-0.0512
Q_{96}	1264.61	0.0581	0.0340	0.0363	0.0358	0.0243	0.0610
Q_{97}	1282.87	-0.0212	-0.0457	-0.0466	-0.0443	-0.0691	
Q_{98}	1285.28	-0.0515	-0.0265	-0.0353	-0.0458	-0.0258	
Q_{105}	1359.54	-0.0423		-0.0301	-0.0324		-0.0499
Q_{108}	1397.31	0.0593	0.0315		0.0764	0.0391	
Q_{111}	1444.50			0.0336			0.0245
Q_{114}	1462.34		0.0572	0.0315	0.0277	0.0431	
Q_{115}	1471.62	-0.0420		-0.0373	-0.0525	-0.0301	-0.0583
Q_{119}	1490.68	0.0326					
Q_{120}	1496.49	-0.0421	-0.0415		-0.0259		
Q_{122}	1534.98	0.0482		0.0436	0.0556	0.0276	
Q_{124}	1541.58	-0.0305	-0.0594	-0.0331	-0.0327	-0.0322	
Q_{125}	1566.85	0.0428	0.1373			0.0450	-0.0778
Q_{126}	1571.67	0.0361	0.1383	0.1029	0.0719	0.1010	0.0291
Q_{128}	1600.42			-0.0274	0.0510	0.0304	-0.1861
Q_{129}	1633.52						

Table S5 Selected inter-state coupling elements $\lambda_i^{(n,m)}$ (in eV and > 0.02 eV) and associated Q_i normal modes and frequencies ω_i (in cm^{-1}).

Complex **1**	ω_i	$\lambda_i^{(S1,S2)}$	$\lambda_i^{(S1,S3)}$	$\lambda_i^{(T1,T2)}$	$\lambda_i^{(T1,T3)}$	$\lambda_i^{(T2,T3)}$
Q_{112}	1390.73	0.0275		0.0259		
Q_{118}	1463.11			0.0267		
Q_{125}	1515.19			0.0212		
Q_{128}	1567.82			0.0251		0.0151
Q_{129}	1573.42		0.0221	0.0424		
Q_{130}	1579.68	0.0381	0.0350	0.0595		
Q_{132}	1585.76	0.0231		0.0238		
Complex **2**	ω_i	$\lambda_i^{(S1,S2)}$	$\lambda_i^{(S1,S3)}$	$\lambda_i^{(T1,T2)}$	$\lambda_i^{(T1,T3)}$	$\lambda_i^{(T2,T3)}$
Q_{85}	1175.72			0.0326		
Q_{96}	1264.61			0.0225		
Q_{97}	1282.87			0.0435		
Q_{98}	1285.28	0.0200		0.0417		
Q_{105}	1359.54			0.0201		
Q_{108}	1397.31			0.0442		
Q_{114}	1462.34			0.0300		
Q_{115}	1471.62			0.0453	0.0200	
Q_{122}	1534.98	0.0209		0.0375		
Q_{124}	1541.58	0.0436		0.0314		
Q_{125}	1566.85	0.0678		0.0603	0.0408	0.0356
Q_{126}	1571.67	0.0716		0.0432	0.0253	
Q_{128}	1600.42		0.0235	0.0550		0.0210

THEORETICAL APPROACHES

1. Formalism developed for MCD within the framework of FFMIO

By defining a laboratory frame in which the $\hat{z}$-axis defines the direction of the light trajectory, circular polarized light interactions can be generated with the use of the complex vectors $\mathcal{E}_{\pm} = \frac{1}{\sqrt{2}}(\hat{x} \pm i\hat{y})$. In this framework the FFMIO operator transforms as:

$$T_{IF}^{\pm} = \frac{1}{\sqrt{2}}\sum_{j=1}^{N}\langle I|e^{-i\mathrm{k}r_j}(\varepsilon \cdot \hat{p}_x)|F\rangle \pm \langle I|e^{-i\mathrm{k}r_j}(\varepsilon \cdot \hat{p}_y)|F\rangle \quad (4)$$

In both ECD and/or CPL spectroscopies, the measured intensities reflect the difference of absorption and/or photoluminescence between the left and right polarized transition moments given by:

$$\Delta_{IF}^{L\pm R}(\mathrm{k},\mathcal{E}) = |T_{IF}^{-}|^2 \pm |T_{IF}^{+}|^2 \quad (5)$$

which leads to the following expressions for the sum and the difference of the square moduli $|T_{IF}^{\pm}|^2$:

$$\Delta_{IF}^{L+R}(\mathrm{k},\mathcal{E}) = \frac{1}{2}\langle I|\sum_{j=1}^{N} e^{-i\mathrm{k}r_j}(\varepsilon \cdot \hat{p}_x)|F\rangle\langle I|\sum_{j=1}^{N} e^{-i\mathrm{k}r_j}(\varepsilon \cdot \hat{p}_y)|F\rangle \quad (6)$$

$$\Delta_{IF}^{L-R}(\mathrm{k},\mathcal{E}) = -\mathbf{Im}\left(\langle I|\sum_{j=1}^{N} e^{-i\mathrm{k}r_j}(\varepsilon \cdot \hat{p}_x)|F\rangle\langle I|\sum_{j=1}^{N} e^{-i\mathrm{k}r_j}(\varepsilon \cdot \hat{p}_y)|F\rangle\right) \quad (7)$$

Performing orientational averaging on expression (7) in presence of a magnetic field and taking into account Zeeman interactions leads to the formulation of MCD expressions in the framework of FFMIO operator.[1]

[1] N. O. Foglia, D. Manganas, F. Neese, J. Chem. Phys. 2022, 157

2. Computational details of the electronic structure calculations

Both ADF[1] and ORCA[2] quantum chemistry software's have been used to generate the electronic structure data exploited subsequently in the quantum dynamics simulations and modelling of the steady-state photophysics and (chiro-) optical properties.

The S_0 electronic ground state structures of **1** and **2** depicted in Scheme 1, have been optimized by means of Kohn-Sham DFT with the B3LYP functional[3,4] with D3 dispersion correction[5] using the all-electrons scheme and a triple-ζ polarized basis set (TZP).[6] TDA approximation was used to treat triplet states. The scalar relativistic effects have been introduced by the zeroth order regular approximation ZORA,[7] the spin-orbit corrections being included as a perturbation. The nature of the stationary state was checked through a complete set of real frequencies. The default value was used for SCF convergence criteria and for the geometry optimization convergence a criteria of 10-4 was employed for the gradient. We requested a verygood quality for the beckegrid integration. All other criteria were the default values of ADF.

The transition energies to the low-lying singlet and triplet excited states have been computed by means of time-dependent DFT (TD-DFT) method[8,9] including solvent corrections for dichloromethane (ε= 8.9, rad =2.94 Å) through the Conductor like screening model (COSMO)[10-12] as implemented in ADF.[13,14] The analysis by TheoDORE, a package for theoretical density, orbital relaxation and excitation analysis.[15] The different computed states are denoted S_x and T_x for x^{th} singlet or triplet states computed without spin-orbit. The "Spin-orbit" states will be denoted E_x.

ORCA code[2] was used specifically for phosphorescence and CPL theoretical spectra calculations. ORCA v5 was used for all the following protocol. ORCA v6 was used only to produce CPL spectra. ORCA calculations were performed at the densi functional theory with B3LYP functional. Resolution of Identity (RI) for the Coulomb and Exchange term with chain of sphere (COS) expansion (RIJCOSX) approximation was introduced to speed up the calculations.[16] All atoms were described with the Def2-TZVP main basis set with def2-TZVP/J and def2-TZVP/C auxiliary basis sets.[17,18] A Douglas-Kroll-Hess 2 Hamiltonian[19,20] was used to introduce relativistic effects for both excited states screening calculations based on TD-DFT method and Excited State Dynamics (ESD) for phosphorescence and CPL spectra. In these cases, a SARC-DKH-TZVP basis set[21] was used instead of DKH-Def2-TZVP for the Pt atom. All calculations were performed with a non-explicit dichloromethane solvent using polarizable continuum model (PCM)[22] as implemented in ORCA.[23] Weak interactions were accounted for using Grimme D3 corrections with Becke-Johnson damping.[5] The default values were employed for the DFT grid with tight and tightopt conv. crit.

[1] ADF2019, SCM, Theoretical Chemistry, Vrije Universiteit, Amsterdam, The Netherlands: https://www.scm.com (DOI: 10.1002/wcms.1606)
[2] Neese, F. Software update: the ORCA program system -- Version 5.0 Wiley Interdiscip. Rev.: Comput. Mol. Sci., 2022, 12, 1, e1606
[3] A. D. Becke, *J. Chem. Phys.* 1993, **98**, 5648-5652.
[4] P. J. Stephens, F. J. Devlin, C. F. Chabalowski, M. J. Frisch, *J. Phys. Chem.,* 1994, **98**, 11623-11627.
[5] S. Grimme, J. Antony, S. Ehrlich, and H. Krieg, J. Chem. Phys. 132 (2010) 154104 ; S. Grimme, S. Ehrlich, and L. Goerigk, J. Comput. Chem. 32 (2011) 1456.
[6] E. van Lenthe, E. J. Baerends, *J. Comp. Chem.* 2003, **24**, 1142-1156.
[7] E. van Lenthe, R. van Leeuwen, E. J. Baerends, J. G. Snijders, *Int. J. Quant. Chem.* 1996, **57**, 281-293.
[8] E. Runge, E. K. U. Gross, *Phys. Rev. Lett.* 1984, **52**, 997.
[9] M. Petersilka, U. J. Gossmann, E.K.U. Gross, *Phys. Rev. Lett.* 1996, **76**, 1212.
[10] A. Klamt, G. Schüürmann, *J. of Chem. Soc.: Perkin Trans*. 1993, **2**, 799-805.
[11] A. Klamt, *J. Phys. Chem*. 1995, **99**, 2224-2235.

[12]A. Klamt, V. Jones, *J. Chem. Phys*. 1996, **105**, 9972-9981.
[13]A. Rosa, E. J. Baerends, S. J. A. van Gisbergen, E. van Lenthe, J.A. Groeneveld, J. G. Snijders, *J. Am. Chem. Soc.* 1999, **121**, 10356-10365.
[14]C. C. Pye, T. Ziegler, *Theo. Chem. Acc.* 1999, **101**, 396-408.
[15] F. Plasser, *J. Chem. Phys*. 2020, **152**, 084108.
[16]F. Neese, F. Wennmohs, A. Hansen, U. Becker, Chem. Phys. 356 (2009) 98. R. Izsak, and F. Neese, JCP 135, 144105 (2011) 144105.
[17]Schäfer, H. Horn, and R. Ahlrichs, J. Chem. Phys. 97 (1992) 2571; F. Weigend, and R. Ahlrichs, Phys. Chem. Chem. Phys. 7 (2005) 3297; A. Schäfer, C. Huber, and R. Ahlrichs, J. Chem. Phys. 100 (1994) 5829.
[18] M. Feyereisen, G. Fitzgerald, and A. Komornicki, Chem. Phys. Lett. 208 (1993) 359; R. A. Kendall, and H. A. Fruchtl, Theor. Chem. Acc. 97 (1997) 158.
[19]M. Douglas, and N. M. Kroll, Ann. Phys. 82 (1974) 89.
[20]B. A. Hess, Phys. Rev. A 33 (1986) 3742.
[21]D. A. Pantazis, X. Y. Chen, C. R. Landis, and F. Neese, J. Chem. Theory Comput. 4 (2008)
908 ; D. A. Pantazis, and F. Neese, J. Chem. Theory Comput. 5 (2009) 2229 ; D. A. Pantazis, and F. Neese, J. Chem. Theory Comput. 7 (2011) 677 ; D. A. Pantazis, and F. Neese, J. Chem. Theory Comput. 7 (2011) 677 ; D. A. Pantazis, and F. Neese, Theor. Chem. Acc. 131 (2012) 1292.
[22]T. N. Truong, and E. V. Stefanovich, Chem. Phys. Lett. 240 (1995) 253 ; R. Cammi, and B. Mennucci, J. Chem. Phys. 110 (1999) 9877.
[23]M. Garcia-Ratés, and F. Neese, J. Comput. Chem. 41 (2020) 922.

3. Construction of the *W(Q)* coupling matrix

Spin-vibronic Hamiltonian in n_{el} coupled diabatic electronic spin-free basis can be expressed as:[1–3]

$$\mathrm{H}(\mathrm{Q}) = (T_N + V_0(\mathrm{Q}))\mathrm{I} + \mathrm{W}^{VC}(\mathrm{Q}) + \mathrm{W}^{SOC}(\mathrm{Q}) \tag{S1}$$

where T_N is the kinetic energy operator of the nucleus, V_0(Q) is the potential energy of some reference electronic state and I is the identity matrix with dimension $n_{el} \times n_{el}$. Here V_0(Q) is determined from the electronic structure calculations at the ground state equilibrium geometry and taken as harmonic potential with vibrational frequencies ω_i along the set of dimensionless normal mode coordinates Q. W^{VC}(Q) is the potential coupling matrix for the vibronic-coupling and W^{SOC}(Q) is the spin-orbit coupling matrix. The W^{VC}(Q) can be expand by Taylor series around the Franck-Condon (FC) point, Q = 0:

$$W_{nn}^{VC}(\boldsymbol{Q}) = \varepsilon_n + \sum_i \kappa_i^{(n)} Q_i + \frac{1}{2}\sum_{ij} \gamma_{ij}^{(n)} Q_i Q_j + \cdots \tag{S2}$$

$$W_{nm}^{VC}(\boldsymbol{Q}) = \sum_i \lambda_i^{(n,m)} Q_i + \cdots \tag{S3}$$

W_{nn}^{VC}(Q) is diagonal matrix element of the W ^{VC}(Q) matrix. ε_n is the vertical excitation energy of the *n*th the electronic state. $\kappa_i^{(n)}$ and $\gamma_{ij}^{(n)}$ are the first and second order intra-state coupling constants for the Q_i mode. In the linear vibronic coupling (LVC) model we will neglect the $\gamma^{(n)}$ and all the higher order terms. On the other hand, W_{nm}^{VC}(Q) is the off-diagonal matrix element with the inter-state coupling constant $\lambda_i^{(n,m)}$. $\kappa_i{}^{(n)}$ can be calculated from the gradient of adiabatic potential energy surface V_n(Q) along Q_i

$$\kappa_i^{(n)} = \frac{\partial V_n(\boldsymbol{Q})}{\partial Q_i}\Big|_0 \tag{S4}$$

$\kappa_i^{(n)}$ represents the force acting within an electronic surface and are responsible for shift in the potential minima for the excited state compared to the ground state minima, they are called tuning modes.

The $\lambda_i^{(n,m)}$ can be computed from the difference between hessian of the two adiabatic sates at FC point.

$$\lambda_i^{(n,m)} = \sqrt{\frac{1}{8}\frac{\partial^2 \left(V_n(\boldsymbol{Q}) - V_m(\boldsymbol{Q})\right)^2}{\partial Q_i^2}}\Big|_0 \tag{S5}$$

$\lambda_i^{(n,m)}$ are responsible for the nonadiabatic transition between two electronic states.

Alternatively, beyond the pair of states approximation, $\lambda\, i^{(n,m)}$ can be evaluated from the overlaps between electronic wavefunctions at close-lying geometries. The W_{nm}^{VC}(Q) matrix in Eq. (S3) can be expresses as

$$W_{nm}^{VC}(\boldsymbol{Q}) = \langle \Phi_n | H_{\mathrm{el}} | \Phi_m \rangle \tag{S6}$$

where H_{el} is the electronic Hamiltonian and Φ_n is the *n*th diabatic electronic state. Consequently, $\lambda_i^{(n,m)}$ can be defined as[4]

$$\lambda_i^{(n,m)} = \frac{\partial W_{nm}^{VC}(\boldsymbol{Q})}{\partial Q_i}\Big|_0 = \frac{\partial \langle \Phi_n | H_{\mathrm{el}} | \Phi_m \rangle}{\partial Q_i}\Big|_0 \tag{S7}$$

For each normal mode *i* of interest, energy $E_n(\delta Q_i)$ of the adiabatic wavefunction $\Psi_n(\delta Q_i)$ is calculated at finite displacement of the geometry δQ_i. Additionally, the overlap between the $\Psi_n(0)$ and $\Psi_n(\delta Q_i)$ is calculated

$$S_i^{nm} = \langle \Psi_n(0) | \Psi_m(\delta Q_i) \rangle \tag{S8}$$

In the realm of TD-DFT, approximate auxiliary many-electron wavefunctions take the form:

$$\Psi_n(\boldsymbol{Q}) = \sum_{ja} X_{ja}^{(n)}(\boldsymbol{Q})\phi_j^a(\boldsymbol{Q}) \tag{S9}$$

Here, $X_{ja}^{(n)}$ represents the TD-DFT response vector element associated with the transition from the occupied orbital *j* to the virtual orbital *a* for state *n*, while ϕ_j^a denotes the corresponding Slater determinant.

Afterwards, an adiabatic-to-diabatic transformation matrix *U* is constructed by a Löwdin orthogonalization[5] of the overlap matrix *S*. The diabatic Hamiltonian at the displaced geome-try is obtained as[6,7]

$$\boldsymbol{W}^{VC}(\delta Q_i) = \boldsymbol{U}\begin{pmatrix} E_1(\delta Q_i) & \cdots & 0 \\ \vdots & \ddots & \vdots \\ 0 & \cdots & E_n(\delta Q_i) \end{pmatrix}\boldsymbol{U}^T \tag{S10}$$

The $\lambda_i^{(n,m)}$ values are computed by a numerical differentiation

$$\lambda_i^{(n,m)} = \frac{\partial W_{nm}^{VC}(\delta Q_i)}{\delta Q_i} \tag{S11}$$

The spin-orbit coupling matrix $W^{SOC}(Q)$ also depends on nuclear coordinates (Q), but for simplicity we take constant value at FC geometry $W^{SOC}(0)$. Spin-orbit coupling causes the radi-ationless singlet-triplet transition. We have considered three singlet states (S_1, S_2, S_3) and three triplet states (T_1, T_2, T_3) to construct the model Hamiltonian for the two complexes **1** and **2**. The $W(Q) = W^{VC}(Q) + W^{SOC}(0)$ can be combinedly written as a 12×12 matrix. Considering the triplet component explicitly W (Q) have the submatrices going from ascending order of magnetic quantum number *m*.

$$W_{nn} = \varepsilon_n + \sum_i \kappa_i^{(n)} Q_i; \quad W_{Sn,Sm} = \sum_i \lambda_i^{Sn,Sm} Q_i; \tag{S12}$$

$$W_{Sn,Tm} = \begin{pmatrix} \eta_{01}^{*Sn/Tm} & \eta_{00}^{Sn/Tm} & \eta_{01}^{Sn/Tm} \end{pmatrix}; \tag{S13}$$

$$W_{Tn,Tm} = \begin{pmatrix} \sum_i \lambda_i^{T1,T3} Q_i + \eta_{11}^{Tn/Tm} & \eta_{01}^{Tn/Tm} & 0 \\ -\eta_{01}^{*Tn/Tm} & \sum_i \lambda_i^{T1,T3} Q_i & \eta_{01}^{Tn/Tm} \\ 0 & -\eta_{01}^{*Tn/Tm} & \sum_i \lambda_i^{T1,T3} Q_i + \eta_{11}^{*Tn/Tm} \end{pmatrix}; \tag{S14}$$

$\eta^{n/m}$ is the spin-orbit coupling constant obtained from the electronic structure calculation using TD-DFT.

$\eta^{Sn/Tm}_{00}$ represent the interaction between S_n (m = 0) and T_m (m = 0) state and $\eta^{Sn/Tm}_{01}$ represent the interaction between S_n (m = 0) and T_m (m = ±1) state. $\eta^{Tn/Tm}_{11}$ represent the interaction between T_n (m = ±1) and T_m (m = ±1) state and $\eta^{Tn/Tm}_{01}$ represent the interaction between T_n (m = 0) and T_m (m = ±1) state. $\boldsymbol{\varepsilon}_n$ is the vertical excitation energy of the spin-free electronic state n.

REFERENCES

[1]J. Eng, C. Gourlaouen, E. Gindensperger, and C. Daniel, "Spin-vibronic quantum dynamics for ultrafast excited-state processes," Account Chem. Res. 48, 809–817 (2015).

[2]T. J. Penfold, E. Gindensperger, C. Daniel, and C. M. Marian, "Spin-vibronic mechanism for intersystem crossing," Chem. Rev. 118, 6975 (2018).

[3]H. Koppel, W. Domcke, and L. S. Cederbaum, "Multimode molecular dynamics beyond the born-oppenheimer approximation," Adv. Chem. Phys. 57, 59–246 (1984).

[4]M. Fumanal, F. Plasser, S. Mai, C. Daniel, and E. Gindensperger, "Interstate vibronic coupling constants between electronic excited states for complex molecules," J. Chem. Phys. 148, 124119 (2018).

[5]P. Löwdin, "On the non-orthogonality problem connected with the use of atomic wave functions in the theory of molecules and crystals," J. Chem. Phys. 18, 365 (1950).

[6]G. Granucci, M. Persico, and A. Toniolo, "Direct semiclassical simulation of photochemical processes with semiempirical wave functions," J. Chem. Phys. 114, 10608 (2001).

[7]F. Plasser, G. Granucci, J. Pittner, M. Barbatti, M. Persico, and H. Lischka, "Surface hopping dynamics using locally diabatic formalism: Charge transfer in the ethylene dimer cation and excited state dynamics in the 2-pyridone dimer," J. Chem. Phys. 137, 22A514 (2012).

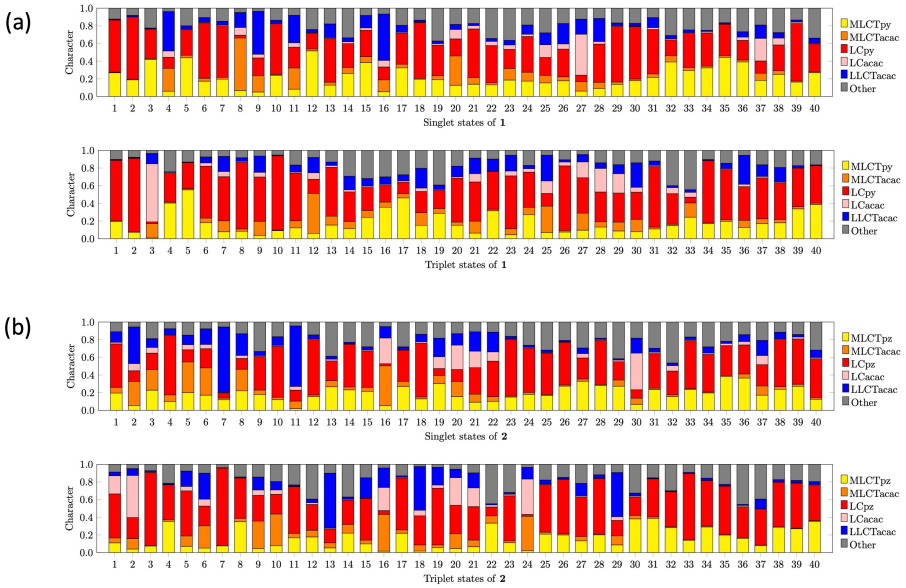

Scheme S1. Electronic structure analysis of the 40 lowest singlet and triplet excited states of complex **1** (a) and complex **2** (b).

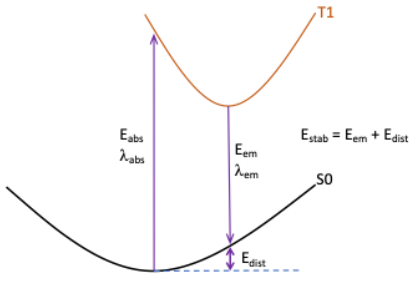

Scheme S2. Definition of E_{dist}, E_{em} and E_{stab} (Table 3).